DC Voltage Control of Single-Stage Isolated AC-DC Converter based on a Half-bridge DAB Converter with PFC capability

Hayate Akiyama[1*], Takashi Ohno[1], Hiroki Watanabe[2], Jun-ichi Itoh[1]
1 Department of Science of Technology Innovation, Nagaoka University of Technology, Nagaoka, Japan
2 Department of Electrical, Electronics and Information Engineering, Nagaoka University of Technology, Niigata, Japan
*E-mail : s243092@stn.nagaokaut.ac.jp

***Abstract*—This paper proposes a DC voltage control method for an isolated AC-DC converter based on a half-bridge Dual Active Bridge (DAB) converter incorporating nonlinear compensation. This paper clarifies the relationship between the phase difference and the output current in each operating mode and the mode identification equation to implement the nonlinear compensation. As a result, the output voltage of the circuit maintains a constant DC voltage even during load variations. The main contribution of this paper is a nonlinear compensation method applicable to a single-stage isolated AC-DC converter based on a half-bridge DAB with an AC input and a continuously varying duty ratio. The experimental results show that the DC voltage fluctuation is limited to 1 V. In addition, the output voltage tracks the reference within 40 μs when the load changes.**

Keywords—DC voltage control, Isolated AC-DC converter, Single stage converter, Power factor correction

I. INTRODUCTION

Recently, high-efficiency and high-power-density AC-DC converters for power adapters have become a major technical trend due to widespread adoption of USB-powered devices [1]-[7]. Power adapters are required to achieve a high efficiency and low total harmonic distortion (THD) of the input current to comply with harmonic regulations and maintain a constant output voltage despite load variations.

A single-stage topology is expected to achieve higher efficiency than a two-stage configuration because it reduces the number of power-conversion stages. In Ref. [8], a single-stage isolated AC-DC converter based on a half-bridge DAB converter has been proposed as a high-efficiency, high power factor converter. This converter achieves Zero-Voltage-Switching (ZVS) capability, power factor correction without the PFC converter, and galvanic isolation by the high-frequency transformer. However, DC voltage control for the converter has not been investigated, and existing studies have been limited to open-loop operation.

In general, the output voltage of the DAB converter is regulated by carrier phase-shift control between the primary and secondary sides. This control inherently involves a nonlinear relationship between the phase difference and the output current. In addition, in the circuit under investigation, the AC input voltage is directly applied to the DAB converter. Therefore, the control system must be designed to avoid interference with the component at twice the input voltage frequency, since the output voltage contains it.

The simplest approach to implementing output-voltage control for the DAB converter is to feed the voltage error into a PI controller and directly use its output as the phase-difference command. However, as mentioned above, the neglect of nonlinear compensation and the inherent limitation of the controller bandwidth may prevent the system from achieving a satisfactory transient response [9]. A control method has also been proposed in which the output current is fed forward to the output of the PI controller [10]. Although this approach provides improved disturbance rejection, the control may still fail because the output of a PI controller, which is the current command, is directly used as the phase-difference command.

To address this problem, a control method has been proposed in which nonlinear compensation is applied to the current command to convert it into the phase-difference command [11]. Implementing this nonlinear compensation term is expected to improve the transient response. However, in the circuit under investigation, multiple operating modes coexist, and the nonlinear compensation equations differ depending on the operating mode. In such cases, a control method has been proposed that detects the operating mode using a mode-identification condition and switches the corresponding nonlinear compensation equations accordingly [12]-[14]. This method allows nonlinear compensation to be properly applied across multiple operating modes. However, implementing a nonlinear compensation approach in the circuit under investigation requires clarifying the relationship between the phase difference and the output current and mode-discrimination equation.

This paper proposes a DC voltage control method with nonlinear compensation for a single-stage isolated AC-DC converter based on a half-bridge DAB converter. The compensation term requires a formulation different from that of conventional DAB converters because the input voltage is AC and the secondary-side duty ratio varies continuously. The new contribution of this paper is a nonlinear compensation method applicable to a single-stage isolated AC-DC converter based on a half-bridge DAB with an AC input and a continuously varying duty ratio, for which conventional DAB compensation methods based on constant DC input assumptions are not applicable. As a result, the output voltage exhibits almost no overshoot during load transients, even though the control bandwidth is limited to avoid interference with the component at twice the input-voltage frequency. Experimental results demonstrate that the proposed method maintains a constant output voltage under load variations.

II. Circuit Configuration and Control

Fig. 1 shows the circuit configuration under investigation. This single-stage AC-DC converter consists of a diode rectifier and a DAB converter. The primary side of the DAB converter employs a half-bridge topology. Thus, the output voltage of the primary side in the DAB converter v_{pri} is a square wave form whose amplitude is half of the input AC voltage v_{ac}. The reg capacitors C_1 and C_2 are implemented with a small capacitance so that the DAB converter is supplied with a full-wave-rectified waveform.

Fig. 2 shows the control block diagram of the circuit. The DC voltage regulation is achieved through the phase-shift control of the primary-side switching carrier. The PI controller is implemented to maintain the commanded DC voltage against load variations. The feedforward compensation of output current I_{dc} helps maintain a constant DC voltage during steady-state operation. There is a nonlinear relationship between the phase difference and the output current. Therefore, a conversion term from the current command to the phase difference is introduced. The nonlinear compensation is achieved by using two conversion equations and switching between them according to the mode identification equation. The switches on the secondary side of the DAB converter are driven by sinusoidal PWM, in which the phase of the modulation waveform is synchronized with the input AC voltage by the Phase-Locked Loop (PLL) to achieve PFC operation.

Fig. 3 shows the operation waveforms of the primary and secondary output voltage of the DAB converter v_{pri}, v_{sec}, and the current flowing through the external inductor i_L. The amplitude of the voltage v_{pri} varies sinusoidally, while the duty ratio is fixed at 0.5. In contrast, the voltage v_{sec} is a constant amplitude at the output DC voltage, but the duty ratio is varied sinusoidally. Therefore, the voltage across the external inductor L becomes sinusoidal, thereby making the relationship between the voltage across L and i_L linear. As a result, PFC operation is achieved without a dedicated PFC circuit. The current i_L is classified into two operating modes depending on the combination of the phase difference and the secondary-side duty ratio.

Fig.4 shows the operation waveforms of each mode in one switching period. The case in which v_{sec} falls before v_{pri} is defined as Mode 1. In this operating mode, the slope of i_L is constant during the on-period of the secondary voltage as in state II of Fig. 4(a). Conversely, the case in which v_{pri} falls before v_{sec} is defined as Mode 2. In this mode, the slope of i_L varies during the on-period of the secondary voltage as in states III and IV of Fig. 4(b). The output current of the DAB converter i_{rec} flows only during the on-period of the voltage v_{sec}. The value of the current i_{rec} is equal to i_L multiplied by the turns ratio N of the high-frequency transformer. The circulating current occurs during the zero voltage intervals as in state I, III, IV and VI of Fig. 4(a) or as in state II and V of Fig. 4(b). The transferred power during that period is dissipated as conduction loss in the switching devices.

Since the relationship between the phase difference and the output current varies across operating modes, nonlinear compensation requires conversion equations specific to each mode. In addition, because these modes coexist during operation, the conversion equations are selected based on the mode identification equation

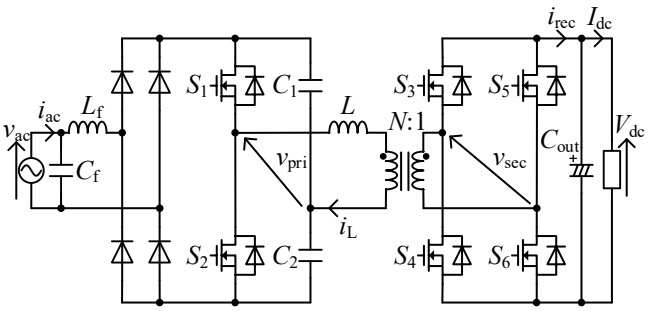

Fig. 1 Circuit configuration

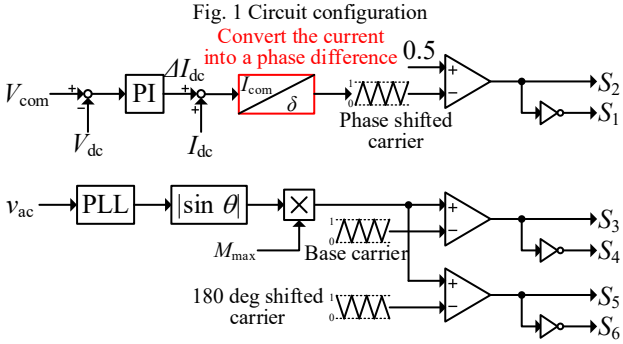

Fig. 2 Control block diagram

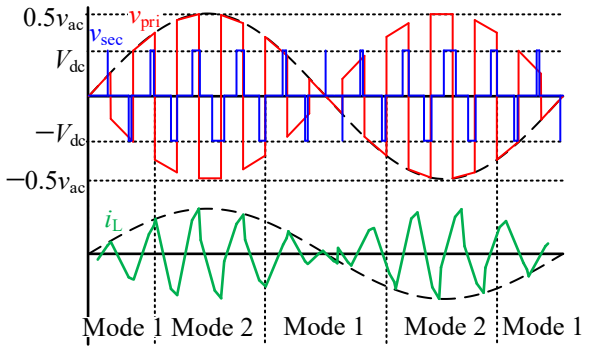

Fig. 3 Operation waveform

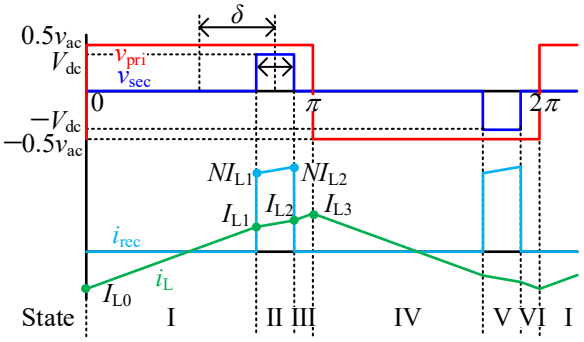

(a) Operation waveform in Mode 1

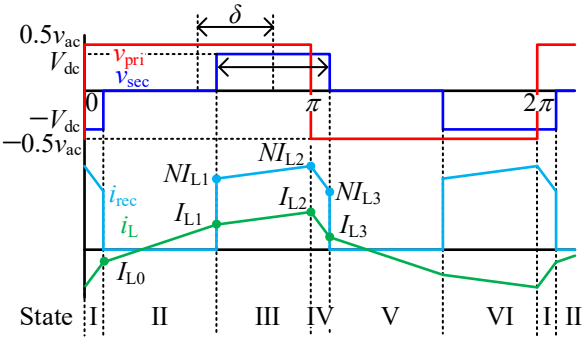

(b) Operation waveform in Mode 2

Fig. 4 Operation waveform of each mode

III. Conversion Equations for Each Mode

The output current I_{dc} corresponds to the DC component contained in the output current of the DAB converter i_{rec}. Therefore, the conversion equations are derived by calculating the average of the i_{rec} in each mode. The current i_{rec} consists of two frequency components, the switching-frequency component and the input AC-frequency component. Therefore, the expression for current I_{dc} is obtained by calculating the average of the current i_{rec} over each frequency component.

The points at which the slope of the current i_L changes in Mode 1 are derived from the voltage across the external inductor L and the duration in each state. The initial current is defined as I_{L0}, the points I_{L1} through I_{L3} in Mode 1 are expressed as

$$I_{L0} = -I_{L3} \tag{1}$$

$$I_{L1} = I_{L0} + \frac{0.5V_{acpeak}\left|\sin\omega_{ac}t\right|}{L}\left\{\left(0.5 - M_{max}\left|\sin\omega_{ac}t\right|\right)\pi + \delta\right\} \tag{2}$$

$$I_{L2} = I_{L1} + \frac{0.5V_{acpeak}\left|\sin\omega_{ac}t\right| - NV_{dc}}{L}2\pi M_{max}\left|\sin\omega_{ac}t\right| \tag{3}$$

$$I_{L3} = I_{L2} - \frac{0.5V_{acpeak}\left|\sin\omega_{ac}t\right| + NV_{dc}}{L}\left\{\left(0.5 - M_{max}\left|\sin\omega_{ac}t\right|\right)\pi - \delta\right\} \tag{4}$$

Similarly, the points I_{L1} through I_{L3} in Mode 2 are expressed as

$$I_{L0} = -I_{L3} \tag{5}$$

$$I_{L1} = I_{L0} + \frac{0.5V_{acpeak}\left|\sin\omega_{ac}t\right|}{L}\left(1 - 2M_{max}\left|\sin\omega_{ac}t\right|\right)\pi \tag{6}$$

$$I_{L2} = I_{L1} + \frac{0.5V_{acpeak}\left|\sin\omega_{ac}t\right| - NV_{dc}}{L}\left\{\left(0.5 + M_{max}\left|\sin\omega_{ac}t\right|\right) - \delta\right\} \tag{7}$$

$$I_{L3} = I_{L2} - \frac{0.5V_{acpeak}\left|\sin\omega_{ac}t\right| + NV_{dc}}{L}\left\{\left(M_{max}\left|\sin\omega_{ac}t\right| - 0.5\right) + \delta\right\} \tag{8}$$

where V_{acpeak} is the peak value of the input AC voltage, L is the external inductance value, δ is the phase difference between the voltage v_{pri} and v_{sec}, M_{max} is the modulation index of the secondary side of the DAB converter, and ω_{ac} is the angular frequency of the grid.

Owing to the symmetry of operation in each half of the switching period, the average value over one full switching period in Mode 1 $i_{1avg,sw}$ is expressed as

$$i_{1avg,sw} = \frac{\delta NV_{acpeak}M_{max}}{2L}\left|\sin\omega_{ac}t\right|^2 \tag{9}$$

In the same way, the average current in Mode 2 $i_{2avg,sw}$ is expressed as

$$i_{2avg,sw} = \frac{NV_{acpeak}}{2L}\left\{\left(1 - \frac{\delta}{\pi}\right)\delta - \left(M_{max}\left|\sin\omega_{ac}t\right| - 0.5\right)^2\pi\right\}\left|\sin\omega_{ac}t\right| \tag{10}$$

The current I_{dc} is obtained by averaging (9) and (10) over the input AC period. By rearranging the equations with respect to δ, the relationship between current I_{dc} and phase difference δ in each mode is expressed as

<Mode 1>

$$\delta = \frac{2\omega_{sw}L}{NV_{acpeak}M_{max}}I_{dc} \tag{11}$$

<Mode 2>

$$\delta = \frac{\pi}{2}\left(1 - \sqrt{\pi M_{max} - \frac{8}{3}{M_{max}}^2 - \frac{4\omega_{sw}L}{NV_{acpeak}}I_{dc}}\right) \tag{12}$$

The solutions in (11) and (12) are selected according to the equation. The equation is derived from the mode boundary condition, at which v_{pri} and v_{sec} fall simultaneously. It is expressed as

$$\begin{cases} \text{Mode}1 : \delta \le \dfrac{\pi}{2}\left(1 - 2M_{max}\left|\sin\omega_{ac}t\right|\right) \\ \text{Mode}2 : \delta > \dfrac{\pi}{2}\left(1 - 2M_{max}\left|\sin\omega_{ac}t\right|\right) \end{cases} \tag{13}$$

The phase difference command is obtained by substituting the current command into I_{dc} in (11) and (12). After performing the calculation, the solution that satisfies (13) is selected and used as the phase difference command. In the controller implementation, the operating mode is identified every switching period based on (13), and the corresponding conversion equation is selected accordingly. No mode-chattering problem was observed in the present experimental conditions.

IV. Experimental Results

Table 1 shows the experimental conditions for verifying the proposed control method. The rated output power of 200 W is defined as 1p.u., and the DC voltage command is set to 24 V. The inductor L_f and the capacitor C_f are used for the input filter to remove the switching frequency component. These values are designed so that the cutoff frequency of the filter is sufficiently lower than the switching frequency.

A. Verification of the DC voltage control method

Fig. 5 shows the steady-state operating waveforms and the transient response under load-step conditions. These experimental results demonstrate that the phase of the input current is synchronized with the input voltage. In addition, the input current exhibits a low-distortion waveform. The THD is 6.3% at 1.0p.u. and 8.3% at 0.5p.u. Under the same conditions, the efficiency is achieved 89.2% at 1p.u. and 91.9% at 0.5p.u. Furthermore, the DC voltage is regulated at 24 V even during load variations, regardless of whether the load steps up or

Table 1 Experiment conditions

Symbol	Quantity	Value
v_{ac}	Grid voltage	200 Vrms
f_{ac}	Grid frequency	50 Hz
V_{dc}	Output voltage	24 V
P_{out}	Output power	200 W
f_{sw}	Switching frequency	50 kHz
M_{max}	Secondary-side modulation index	0.30
L	External inductance	38 μH
N_1:N_2	Number of turn	66:10
L_{leak}	Leakage inductance	48 μH
L_f	Input filter inductor	1.2 mH
C_1,C_2	Arm capacitor	0.47 μF
C_{out}	Output capacitor	10.8 mF
C_f	Input filter capacitor	0.33 μF

down. From the transient waveforms during load variations, the DC voltage deviation is limited to 1 V, and the output voltage returns to the reference within 40 μs. Despite intentionally keeping the control bandwidth low to avoid interference with the component at twice the input voltage frequency contained in the DC voltage, the DC voltage exhibits almost no overshoot during load transients.

B. The Influence of the Modulation Index

Fig. 6 shows the input-current waveforms for different modulation indices. Note that the input voltage in this experiment is set to 230 V_{rms}. When the modulation index is set to 0.5, a current distortion appears around the peak of the current i_{ac}. Under this condition, the THD of the input current is 6.6%. On the other hand, the distortion is reduced when the modulation index is set to 0.369, and the THD of the input current is reduced to 4.2%.

Fig. 7 shows the inductor current waveform around the input voltage peak. The highlighted point represents the condition under which the current I_{L3} is most likely to become negative. This occurs because the applied voltage across the inductor L is the maximum, resulting in the steepest slope of i_L, and the duration of this state is the longest because the secondary side duty ratio is maximized. Fig. 7 (a) shows the inductor current waveform when the modulation index is set to 0.5. In this case, the current i_L becomes negative when the voltage v_{sec} falls. However, Fig. 7 (b) shows the waveform when the modulation index is set to 0.369. In this case, the current i_L crosses zero even in the region where it is most likely to become negative.

Fig. 8 shows the harmonic analysis results of the input current for different modulation indices. In this result, the fifth and ninth order harmonics are especially reduced, by 61% and 81%, respectively. This result also indicates that the smaller modulation index leads to an input current waveform with less distortion.

Fig. 9 shows the RMS value of the inductor current for different modulation indices. The RMS value with a modulation index of 0.2 is higher than that with a modulation index of 0.369 in the output power range from 0.25p.u. to 1.0 p.u., due to the increased zero voltage period. The high RMS current leads to increased conduction loss.

Fig. 10 shows the efficiency comparison with respect to the modulation index. Operating at a higher modulation index achieves higher efficiency regardless of input voltage.

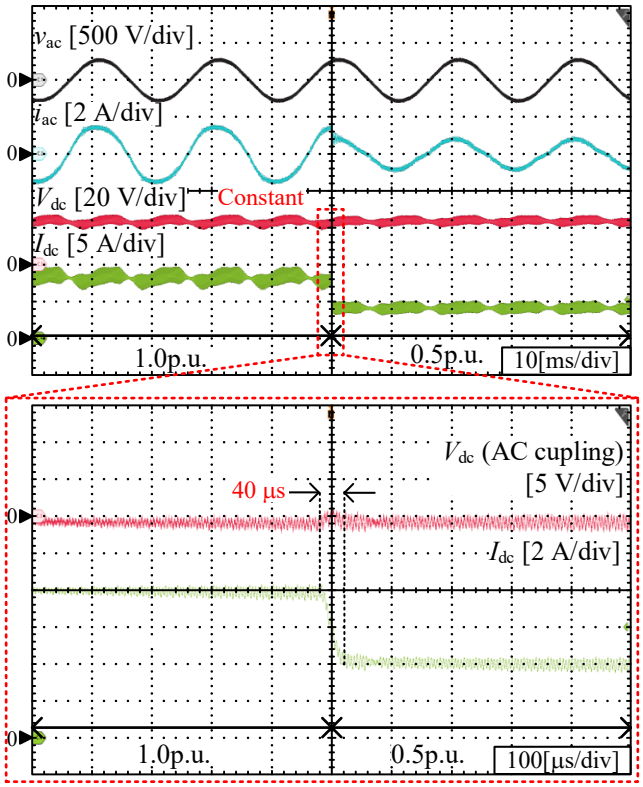

(a) The output power is changed from 1.0p.u. to 0.5p.u.

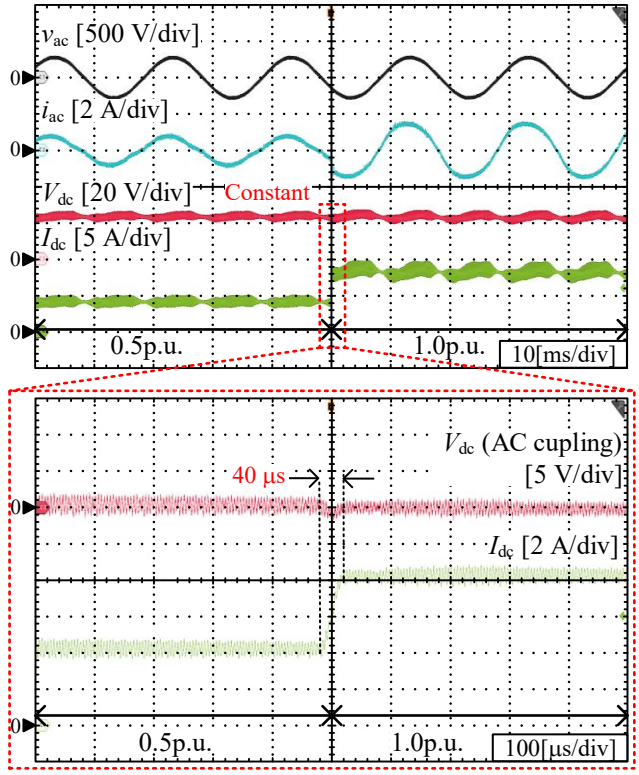

(b) The output power is changed from 0.5p.u. to 1.0p.u.

Fig. 5 The load variations response controlled by the proposal method

From the results of Fig. 8, Fig. 9 and Fig. 10, there is a tradeoff between the efficiency and the THD of the input current. The design method for the modulation index M_{max} has been proposed in Ref. [8]. The design method is able to minimize both the loss and the input current THD. However, the design method is available only under the fixed phase difference. The proposed control method actively adjusts the phase difference to stabilize the DC voltage. The design

method of the modulation index M_{max} under the DC voltage control conditions remains a subject for future investigation.

V. Conclusions

This paper has proposed a DC voltage control method for the single-stage isolated AC-DC converter based on a half-bridge DAB converter. The conversion equations that relate the current command to the phase difference for each operating mode, along with the mode identification equation, are derived to implement nonlinear compensation. The experimental results show that the DC voltage exhibits almost no overshoot during load variations, despite intentionally keeping the control bandwidth low to avoid interference with the component at twice the input voltage frequency contained in the DC voltage. In addition, the proposed control method achieves a settling time of 40 μs. The validity of the proposed control method was confirmed through these experiments.

References

[1] K. H. Cheng, T. J. Liang, H. K. K. Nghiep, K. H. Chen, "Design and Implementation of Asymmetric Half-Bridge Flyback Converter for USB Power Delivery Applications", 2023 11th International Conference on Power Electronics and ECCE Asia (ICPE 2023 - ECCE Asia), 2023, pp.593-600

[2] Y. Chen, Y. F. Liu, "Power Adapter with Line Voltage Control for USB Power Delivery", 2019 IEEE Applied Power Electronics Conference and Exposition (APEC), 2019, pp.2054-2060.

[3] A. M. Garcia, M. Krueger, M. Schmid, J. Daimer, M. Schlenk, "Hybrid-flyback and GaN enable ultra-high-power density 240W USB-PD EPR adaptor", 2023 IEEE Applied Power Electronics Conference and Exposition (APEC), 2023, pp.1259-1264.

[4] Z. Ma, Y. Lai, Q. Huang, Y. Yang, S. Wang, "Investigation and Mitigation of Radiated EMI due to Near-field Coupling in a High-density Active-clamp Flyback Power Adapter", 2023 IEEE Energy Conversion Congress and Exposition (ECCE), 2023, pp.2953-2958.

[5] S. Dey, M. B. Ray, H. Soni, R. Ghosh, M. Shah, "Comparison between Quasi-Resonant and Active Clamp Flyback topologies for GaN-based 65W Wall Charger Application", 2021 IEEE Applied Power Electronics Conference and Exposition (APEC), 2021, pp.1809-1814.

[6] X. Tian, H. Cui, L. Xue, "Multiplexing-Based Flyback Converter for Multi-Port USB Power Delivery with True Power-Sharing", 2021 IEEE Energy Conversion Congress and Exposition (ECCE), 2021, pp.2048-2054.

[7] H. Li, S. Li, W. Xiao, S. Y. R. Hui, "A Modulation Method for Capacitance Reduction in Active-Clamp Flyback-Based AC–DC Adapters", IEEE Transactions on Power Electronics, Vol. 37, No.8, pp. 278-283, Aug. 2022

[8] H. Watanabe, J. Itoh, N. Izumoto, K. Kidera, K. Okada, "High-Efficient Isolated AC-DC Converter with Circulating Current Reduction for AC Adapters", PCIM Europe 2024; International Exhibition and Conference for Power Electronics, Intelligent Motion, Renewable Energy and Energy Management, 2024, pp.3120-3124

[9] H. Qin, J. W. Kimball, "Closed-Loop Control of DC–DC Dual-Active-Bridge Converters Driving Single-Phase Inverters", IEEE Transactions on Power Electronics, IEEE Transactions on Power Electronics, Vol. 29, No. 2, Feb. 2014

[10] S. Shao, L. Chen, Z. Shan, F. Gao, H. Chen, D. Sha, "Modeling and Advanced Control of Dual-Active-Bridge DC–DC Converters: A Review", IEEE Transactions on Power Electronics, Vol. 37, No. 2, Feb. 2022

[11] A. Tong, L. Hang, G. Li, J. Huang, "Nonlinear characteristics of DAB converter and linearized control method", 2018 IEEE Applied Power Electronics Conference and Exposition (APEC), 2018, pp. 331-337

[12] D. Nguyen, D. T. Nguyen, G. Fujita "New Modulation Strategy Combining Phase Shift and Frequency Variation for Dual-Active-Bridge Converter," IEEJ Journal of Industry Applications, vol. 6, No. 2, pp. 140-154, 2017

[13] T. Mishima, Y. Koga, "Variable Frequency Phase-Shift Modulation Symmetrical Series-Resonant Bidirectional DC-DC Converter—Analysis and Verification of ZVS Performance and Reactive Power Minimization—" IEEJ Journal of Industry Applications, vol. 10, No. 5, pp. 540-553, 2021

[14] K. Kawauchi, H. Watanabe, J. Itoh, "Transmission Power Error Compensation Method of Dual Active Bridge Converters under DC-bus Voltage Fluctuation", IEEJ Journal of Industry Applications, Vol. 15, No.1, pp. 54-67, 2026

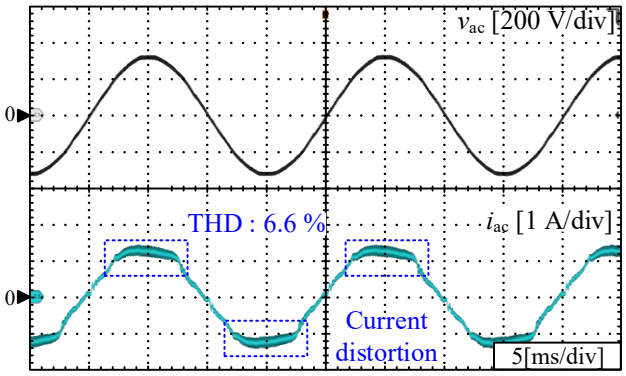

(a) M_{max} = 0.5

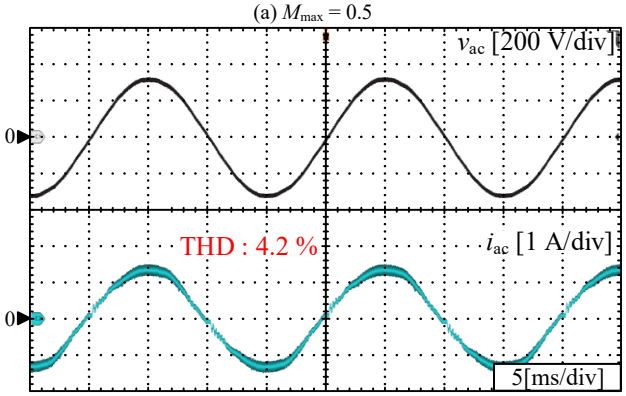

(b)M_{max} = 0.369

Fig. 6 The input current distortion depending on the modulation index

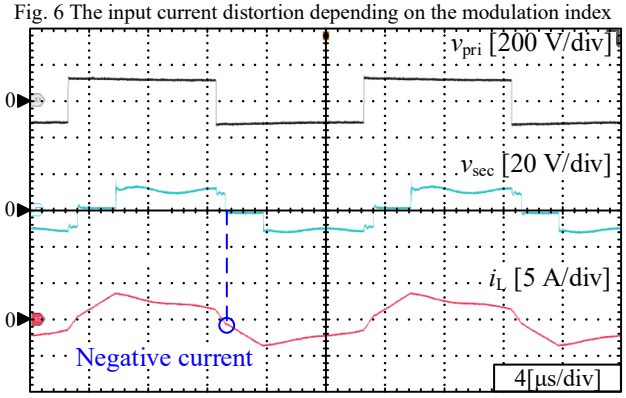

(a) M_{max} = 0.5

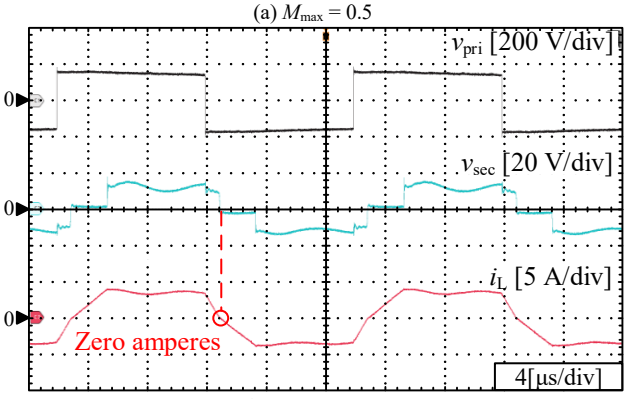

(b) M_{max} = 0.369

Fig. 7 The inductor current waveform around the input voltage peak

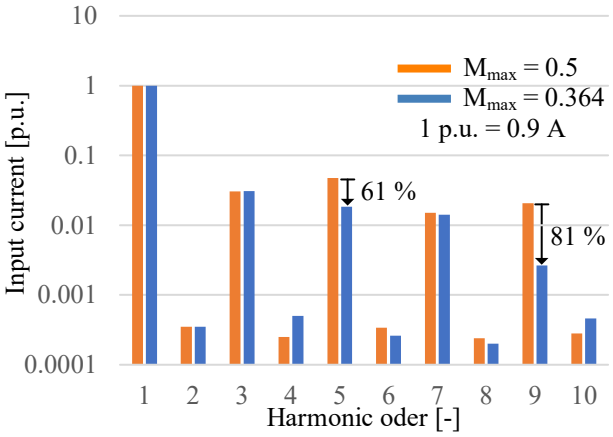

Fig. 8 The harmonic analysis of the inductor current regarding the modulation index

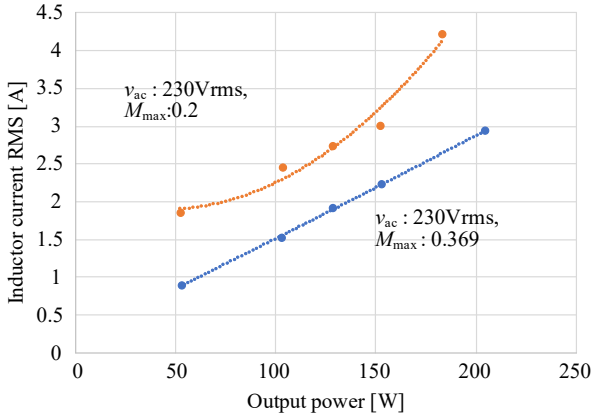

Fig. 9 The RMS value of the inductor current regarding the modulation index.

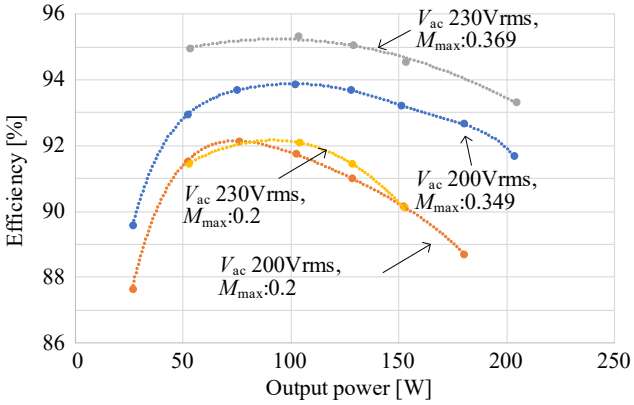

Fig. 10 Efficiency comparison with respect to modulation index